Journal of Power Sources 445 (2020) 227280

Contents lists available at ScienceDirect

Journal of Power Sources

journal homepage: www.elsevier.com/locate/jpowsour

Short communication

Efficient oxygen reduction activity on layered palladium phosphosulphide and its application in alkaline fuel cells

Sujoy Sarkar, Shubham Patel, S. Sampath *

Department of Inorganic and Physical Chemistry, Indian Institute of Science, Bangalore, 560012, India

HIGHLIGHTS

- A ternary layered PdPS is employed as a catalyst for ORR in alkaline medium.
- The ORR is found to occur through a direct four electron pathway.
- PdPS has been used as cathode catalyst in anion exchange membrane fuel cell.
- A peak power density of 340 $mWcm^{-2}$ at 60 °C is observed for the AEMFC.
- Performance in fuel cell is quite comparable to that of Pt/C under similar conditions.

GRAPHICAL ABSTRACT

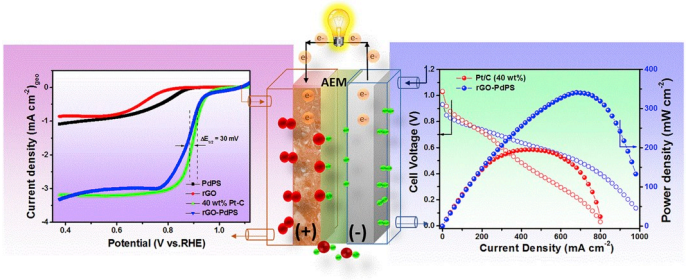

ARTICLE INFO

Keywords:
Palladium phosphosulphide
Oxygen reduction reaction
Anion exchange membrane fuel cell
Electrocatalyst

ABSTRACT

Metal chalcogenides-based electrocatalysts have received considerable attention in recent years. Herein, a layer-type ternary chalcogenide compound, PdPS is proposed as an efficient oxygen reduction reaction electrocatalyst in alkaline medium. PdPS is semiconducting that crystallizes in orthorhombic symmetry. Improvement in conductivity of PdPS using reduced graphene oxide results in excellent electrocatalytic activity. The kinetics is followed by rotating (ring) disk electrode measurements and the composite electrocatalyst is found to be stable, efficient and methanol tolerant. The catalyst is further used as cathode in anion exchange membrane fuel cell and is shown to deliver power density comparable to Pt/C catalyst. In addition, this catalyst is also capable of water oxidation from alkaline solution with favorable electrochemical parameters.

1. Introduction

In view of the increasing energy consumption and levels of greenhouse gases, there is a need for alternative energy sources that will be used to provide clean and environmentally friendly solutions [1]. Fuel cells [2,3] have been prescribed as alternative energy systems for several years but suffer from certain problems associated with sluggish kinetics of ORR that limits their performance [4–6]. Alkaline fuel cell (AFC) that uses aqueous KOH as the electrolyte, overcomes the problems to certain extent, but still improvements are necessary both in the membrane as well as in the catalyst components to achieve good performance [7,8].

Platinum as well as non-Pt based catalysts have been reported for ORR in the literature [9–11]. Among the non-Pt electrocatalysts, transition metals [12,13], metal carbides [14,15], oxides [16], nitrides [17,18] have been well explored. Metal chalcogenides (M_aX_b, M = Mo, Co, Ru, Fe, Ni etc, X = S, Se,Te) have been recognized as promising candidates owing to their potential in electrochemical energy conversion and storage systems [19–24]. Chalcogenides are very often tolerant to

* Corresponding author.
E-mail address: sampath@iisc.ac.in (S. Sampath).

https://doi.org/10.1016/j.jpowsour.2019.227280
Received 9 May 2019; Received in revised form 4 October 2019; Accepted 8 October 2019
Available online 24 October 2019

methanol [21]. Efforts have also been invested to modify chalcogenides using different carbon-based materials [22,25], to form composites. Wang et al. [25] synthesized cobalt sulfide/graphene composite and have shown efficient electrocatalysis for ORR in alkaline medium. Sahu et al. reported metal sulphide (Mo, Co and Mn) [26–28] - graphene composites as efficient ORR catalyst and evaluated their performance in AEMFCs environment.

In the present study, we have explored a ternary layered phosphochalcogenide, palladium phosphosulphide (PdPS) as an efficient electrocatalyst for ORR in alkaline medium. Further, we have demonstrated its use in alkaline fuel cells with favorable characteristics. Though PdPS has been synthesized and studied quite early in the literature [29,30], electrocatalysis on PdPS has only recently been explored. As part of our research efforts towards energy related applications [31–34], hydrogen evolution activity on PdPS has been shown to be better than several chalcogenide-based catalysts. Herein, we show PdPS and its graphene composite as active electrocatalyst towards ORR in alkaline medium. The half-wave potential is quite comparable to the state-of-the-art material, i.e. Pt/C. Further, the PdPS is employed as cathode catalyst in alkaline fuel cell and the power density observed is fairly high (341 $mWcm^{-2}$). To the best of our knowledge, this is the first report where a phosphosulphide composite is used as a catalyst in a fuel cell device with performance higher than that of other reported metal chalcogenide-graphene based composites [26–28].

2. Experimental section

2.1. Synthesis of PdPS and its rGO composite

Synthesis of palladium phosphosulphide, PdPS and its graphene composites are based on previously reported literature from our group [31]. Briefly, precursor materials (Pd, P and S) in their pure elemental form were taken in 1:1:1 atomic ratio in a clean quartz tube and sealed under vacuum at a pressure of $\sim 10^{-6}$ mbar. The sealed tube was kept in a tubular furnace at 950 °C for 7 days. The silver shiny and single-phase crystals were found to be deposited on the inner walls of the tube. Large sized graphene oxide nanosheets were prepared using modified Hummers' method [35]. The composite (rGO-PdPS) was prepared [31] by mixing 20 mg of PdPS with 20 mL aqueous slurry of graphene oxide (1 $mgmL^{-1}$) and sonicating the colloid for 30 min to form a homogeneous dispersion. The slurry was transferred to a Teflon lined autoclave which was heated to 180 °C for 20 h and subsequently cooled, washed with distilled water and dried.

2.2. Characterization

The material characterization involving PdPS and rGO-PdPS composite was based on various techniques as given earlier [31]. Electrochemical measurements were carried out in three-electrode electrochemical cell using a potentiostat/galvanostat (CHI 660A, CH Instruments, USA). Rotating disc electrode (RDE) and rotating ring-disk electrode (RRDE) measurements were performed using RRDE set up (Model AFM, SRCE Pine instruments, USA). A pre-calibrated MMO reference electrode [36] was used for the measurements and all the potentials are referred to RHE according E (RHE) = E (MMO) + 0.975 V. The fuel cell fabrication procedure has been discussed in detail in supporting information.

3. Results and discussion

Physicochemical characterization (Fig. S1) of pristine PdPS and its graphene composite has been extensively carried using various techniques and the material is found to be highly crystalline with pure single phase as observed in our previous studies [31].

3.1. Oxygen reduction reaction

The electrocatalytic ORR activity of pristine PdPS and rGO-PdPS composites were followed by recording voltammograms in 1 M KOH electrolyte saturated with N_2 and O_2 at a scan rate of 10 mVs^{-1}. In the case of bulk PdPS, the ORR peak is centered at 0.65 V vs. RHE in O_2 saturated solution (Fig. 1a). The oxygen reduction peak shifts to 0.81 V for the rGO-PdPS composite (Fig. 1b), under identical conditions. A shift of 160 mV towards the positive potential value along with almost one order increase in cathodic current implies facile ORR reduction when rGO is present along with PdPS.

Further, the ORR kinetics is elucidated using rotating disk electrode (RDE) measurements from the Koutecky-Levich (K-L) equations (Supporting Information [37]). Fig. 1c shows the voltammograms at different rotation rates, from 200 to 2000 rpm, at a scan rate of 5 mVs^{-1}. For comparison, conventional catalyst 40 wt% Pt/C and bulk PdPS are also shown (Fig. S2). It is found that limiting current densities increase with the rotation rates as expected for a convective diffusion process. K-L plots between the inverse of kinetic current (j_k^{-1}) vs. inverse of square root of rotation rate ($\omega^{-1/2}$) are shown in Fig. 1d. The plots reveal nearly parallel lines, implying first order reaction kinetics towards the concentration of dissolved O_2 [38–40]. The number of electrons transferred is determined to be 3.6–3.9 in the potential range, 0.35 V–0.65 V (inset of Fig. 1d), suggesting that rGO-PdPS composite favors a 4e− process, similar to ORR catalyzed by 40 wt% Pt-C (Fig. S2d). However, two electron reduction is the dominant reaction pathway for pristine PdPS as inferred from Figs. S2a and b. The electrochemical rate constant (k) value for rGO-PdPS composite is determined to be 1.96×10^{-2} cms^{-1} at 0.675 V vs RHE (Table S2) while it is 5.69×10^{-2} cms^{-1} on 40 wt% Pt-C at the same dc bias potential.

The determination of the ORR pathway can be established using RRDE experiments where the H_2O_2 produced at the disk is analyzed on the ring and thus ring current density is a direct measure of peroxide produced. The RRDE plot is displayed in Fig. 1e where rGO-PdPS composite electrode is swept at 5 mVs^{-1} scan rate and at 1600 rpm in O_2-saturated 1 M aqueous KOH solution. The ring potential is kept at 1.475 V vs RHE. Disk current and ring current versus.

Applied potential at different rotation speeds are shown in Fig. S3. The number of electrons transferred during ORR is determined to be 3.4–3.8 over the potential range 0.35–0.7 V. This is in parallel to the results obtained from the K-L plots based on RDE studies (Fig. 1d), implying that the rGO-PdPS catalyst reduces molecular oxygen to OH^- through favorable four electron transfer in the diffusion controlled kinetic region. The voltammetric data shown in Fig. S3 is used to calculate the percentage of H_2O_2 formed during ORR. It is found that the percentage of H_2O_2 formed during the course of ORR is ~20–25% in the potential range of 0.375–0.675 V (Table S2), which implies the involvement of two coexisting pathways, viz., where O_2 is first reduced into H_2O_2 and further to OH^- according to the equations given below.

$$\text{One step four-electron pathway: } O_2 + 2H_2O + 4e^- \rightarrow 4OH^- \quad (1)$$

$$\text{Two step two-electron pathway: } O_2 + H_2O + 2e^- \rightarrow HO_2^- + OH^- \quad (2)$$

$$H_2O^- + H_2O + 2e^- \rightarrow 3OH^- \quad (3)$$

Fig. 2a compares the voltammetric behaviour on different catalysts including rGO, PdPS, rGO-PdPS composite and 40 wt% Pt-C modified GC electrode in O_2-saturated 1 M KOH solution at 1600 rpm rotation rate. The half-wave potential ($E_{1/2}$) observed on rGO-PdPS is 30 mV more negative than that observed on Pt/C, thus indicating that the composite of layered PdPS with rGO is an efficient ORR catalyst. The ORR parameters such as onset potential (E^{on}), half-wave potential ($E_{1/2}$) and kinetic current density (i_k @ 0.8 V vs RHE) are determined for all electrocatalysts and tabulated in Table 1. The Tafel plots are shown in Fig. 2b (Table 1). reveals two slopes that arise due to adsorbed –OH species. A change in slope at high (b1) and low over potential (b2)

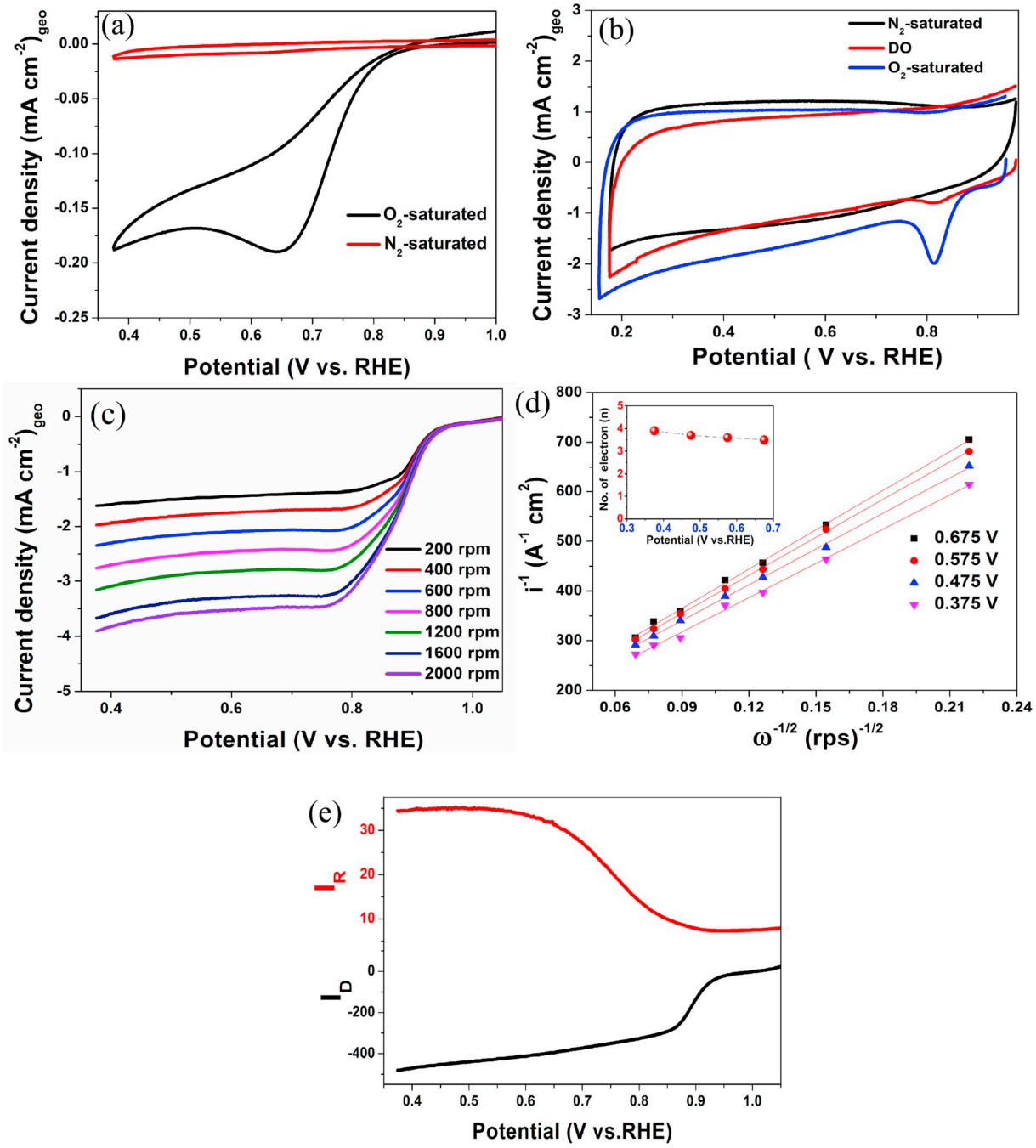

Fig. 1. (a) Cyclic voltammograms of bulk PdPS composite for ORR in presence of N_2-saturated, O_2-saturated 1 M KOH solution at 10 mVs^{-1} scan rate. (b) i-v curves on rGO-PdPS composite in N_2-saturated, dissolved oxygen (DO) and O_2-saturated 1 M KOH at 10 mVs^{-1} scan rate. (c) RDE voltammograms of rGO-PdPS in O_2-saturated 1 M KOH at sweep rate 5 mV^{-1} at different rotation speed as indicated. (d) Corresponding K-L plots at different potentials. Inset shows the number of electrons transferred at different potentials. (e) RRDE voltammograms on rGO-PdPS in O_2-saturated 1 M KOH at 1600 rpm. The disk potential is scanned at 5 mVs^{-1} and ring potential is fixed at 1.475 V vs RHE. The upper half of the voltammogram shows ring current, denoted as i_R while the lower half of the voltammogram shows disk current, denoted as i_D.

regions is due to a shift from Temkin to Langmuir adsorption behaviour of reaction intermediates [41]. A slope of 120 $mVdec^{-1}$ in the kinetically controlled region implies 4e transfer during O_2 to OH conversion. At high over potentials, the observed Tafel slopes are 63.3 and 56.7 $mVdec^{-1}$ on rGO-PdPS and Pt/C respectively. In the kinetic controlled region, the slopes are observed to be 121.2 and 118.4 $mVdec^{-1}$for rGO-PdPS and Pt/C, respectively.

3.2. Methanol tolerance

In addition to the ORR activity of the catalyst, a high catalytic selectivity against fuel oxidation is one of the major concerns for employing in practical alcohol fuel cell. Particularly, when methanol is used as a fuel, it could cross over from anode to cathode. Therefore, methanol tolerance study is important for any new ORR catalyst since it could be useful in direct methanol fuel cells as well. Due to cross-over of the methanol through the membrane, the ORR cathode is exposed to methanol and in the case of Pt, the performance is affected adversely.

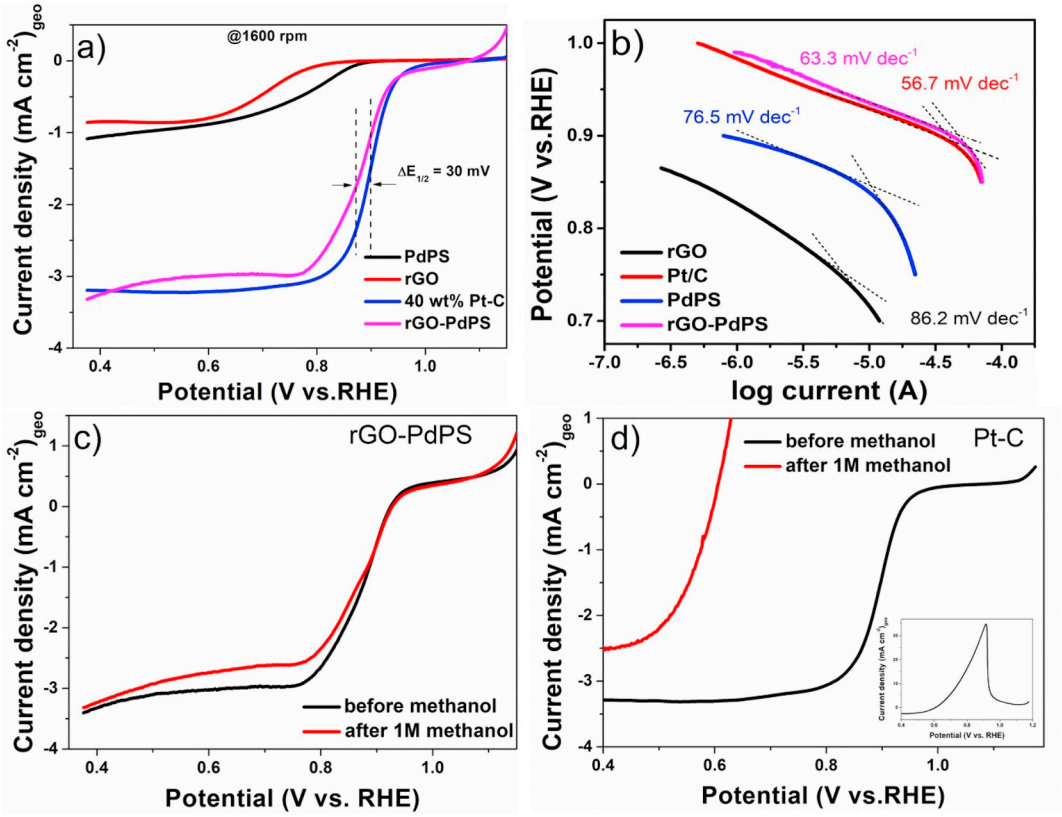

Fig. 2. (a) Comparative rotating disk voltammograms studies with rGO, bulk PdPS, rGO-PdPS and 40 wt% Pt-C in 1 M KOH at 1600 rpm rotation speed. The voltammogram is swept at 5 mVs^{-1} sweep rate. (b) Tafel plots of rGO, PdPS, rGO-PdPS and 40 wt%Pt-C in 1 M KOH solution at 1600 rpm rotation speed. Methanol crossover study of (c) rGO-PdPS and (d) Pt/C with an electrode rotation rate of 1600 rpm at and a scan rate of 5 mVs^{-1} 1 M methanol was added into 1 M KOH electrolyte to evaluate the crossover effect. Inset shows the methanol oxidation by Pt/C.

Table 1
Oxygen reduction parameters including onset potential, half-wave potential, kinetic current density and Tafel slopes for different catalysts (rGO, PdPS, rGO-PdPS and 40 wt% Pt-C) in O_2-saturated 1 M KOH at 5 mVs^{-1} sweep rate. The rotation speed of the electrode used is 1600 rpm.

Electrocatalyst	Onset potential (E^{on}/V vs RHE)	Half-wave potential ($E_{1/2}$/V vs RHE)	Kinetic current density (i_k/ $mAcm^{-2}$) @ 0.8 V vs RHE	Tafel slope ($mVdec^{-1}$)	
				B1	b2
rGO	0.79	0.70	0.32	86.2	160.6
PdPS	0.85	0.78	1.94	76.5	135.4
rGO-PdPS	0.94	0.87	8.23	63.3	121.2
Pt/C	0.94	0.90	31.5	56.7	118.4

The ORR activities of Pt/C and rGO-PdPS catalyst are measured in presence of 1 M methanol at 1600 rpm and depicted in Fig. 2(c,d). In the case of Pt/C, methanol is oxidized (inset of Fig. 2d) under the applied potential range, which is reflected from the high current density values (Fig. 2d). On the contrary, rGO-PdPS shows hardly any change in the current density, implying very good methanol tolerant behavior.

The stability of the catalyst towards ORR is assessed using chronoamperometry wherein the catalyst is kept at a constant potential (0.8 V vs RHE). The percentage of normalized current density with respect to initial current (Fig. S4) reveals that ~80% activity is retained in the case of rGO-PdPS after ~5 h of continuous operation, while it drops to 50% in the case of Pt/C under identical conditions. For comparative purposes, it should be pointed out that the heteroatom-doped rGO supported $NiCo_2S_4$ catalyst has been reported to show good stability with time [42].

The good catalytic behavior of rGO-PdPS composite towards ORR may be due to the following reasons. First, electronic conductivity of the composite improves when rGO is used along with the semiconducting PdPS, thus paving way for good electron transport. Second, the four electron transfer pathway for rGO-PdPS compared to the two electron pathway for pristine PdPS may be due to the presence of rGO sheets which possibly serve as a "peroxide cleaner" [43]. The contribution from the phosphorous – carbon (P-C) and sulphur – carbon (S-C) interactions cannot be overlooked as P- doped graphene [44,45] and S- doped graphene [46] are known to be good catalysts towards ORR. To understand the synergistic coupling and involvement of interaction between PdPS and rGO prepared using hydrothermal process, physical mixture of PdPS and rGO is used as a catalyst and the ORR activity is compared under similar conditions (Fig. S5). The high on-set potential and low current density observed in the case of the physical mixture reveals that the composite possesses favorable interactions between rGO and PdPS. The surface of the catalyst is examined using XPS (Fig. S6). The high resolution P−2p core level spectrum reveals an additional broad peak at ~133.2 eV which is assigned to P–O type functional groups [47]. The peak is assigned to partially oxidized P that might exist in different forms such as C_3PO_2, C_3PO and CPO_3 [44]. Due to high electronegativity of oxygen, P gets polarized creating charge on the adjacent carbon by withdrawing electrons. As a result, positively charged carbon species becomes an active site for O_2 adsorption. This weakens the O–O bond thus facilitating the reduction of O_2 to OH^-. This interaction between P and rGO possibly happens during the hydrothermal process.

3.3. Fuel cell performance

Based on various physical characterization and electrochemical studies, it is found that the rGO-PdPS composite catalyst exhibits very good performance towards oxygen reduction reaction in alkaline

medium. Therefore, the catalyst is tested in alkaline fuel cell where membrane electrode assembly (MEA) is fabricated by employing rGO-PdPS as cathode catalyst.

A catalyst loading of 40% rGO-PdPS/C is optimized by varying the catalysts amount and following the polarization behavior. The effect of cathode catalyst loading on power density is shown in Fig. 3a where the anode catalyst loading is kept constant at 0.8 $mg_{Pt}cm^{-2}$ using 40 wt% Pt-C. The effect of polarization curves with current density at different rGO-PdPS loadings is shown in Fig. S7. It is found that an increase of rGO-PdPS catalyst loading results in an increase in the power density up to 1.4 $mgcm^{-2}$ of the composite (PdPS loading is 0.7 $mgcm^{-2}$) after which the power density starts to decrease with further increase in active material loading.

The fuel cell performance characteristics are investigated at different temperatures and depicted in Fig. 3b where the polarization behavior and the power density profiles are shown for the fuel cell employing 1.4 $mgcm^{-2}$ rGO-PdPS and 0.8 $mg_{Pt}cm^{-2}$ Pt as cathode and anode loadings at 40 °C, 50 °C and 60 °C in presence of humidified H_2 and O_2 gases under ambient pressure. It is found that cathode loading of 1.4 $mgcm^{-2}$ results in the highest power density of 341 $mWcm^{-2}$ at 60 °C without any back pressure. The obtained power density for rGO-PdPS cathode catalyst is higher than the reported chalcogenide-graphene composites [26–28].

The obtained results are compared with Pt/C, employing 0.8 $mg_{Pt}cm^{-2}$ as catalyst for both anode and cathode, which results in a maximum power density of 194 $mWcm^{-2}$ at 60 °C (Fig. 3c) following identical fuel cell testing conditions. The difference in the performance could be due to active surface area of the catalyst. Nevertheless, the fuel cell performance for the phosphosulphides may open up a new direction to develop an efficient and novel electrocatalyst for Pt-free fuel cell.

3.4. Oxygen evolution reaction (OER)

It is noteworthy that apart from ORR, rGO-PdPS is able to oxidize water from the alkaline medium. The OER polarization plot of the rGO-PdPS electrode measured in 1 M KOH solution at a scan rate of 5 mVs^{-1} is depicted in Fig. 4. As observed, rGO-PdPS is indeed very active for OER. The potential required to achieve 10 $mAcm^{-2}$ current density, which is very often used a performance indicator of the catalyst for OER activity [48] is found to be, $\eta = 0.57$ V. The overpotential value is comparable to several oxide based OER catalysts [36,49]. It should be pointed out that chalcogenide catalysts undergo oxidation and an oxide, oxyhydroxide layer is formed prior to OER [50]. The overall elctrocatalytic activity and reversibility of rGO-PdPS as an oxygen electrode in alkaline medium is estimated based upon the potential difference between ORR and OER. The value of the oxygen electrode activity ($\Delta E = E_{j=10\ mA\ cm\text{-}2} - E_{j=3\ mA\ cm\text{-}2}$) [48] for the present catalyst is 0.97 V which reveals the bi-functional behavior of rGO-PdPS for ORR

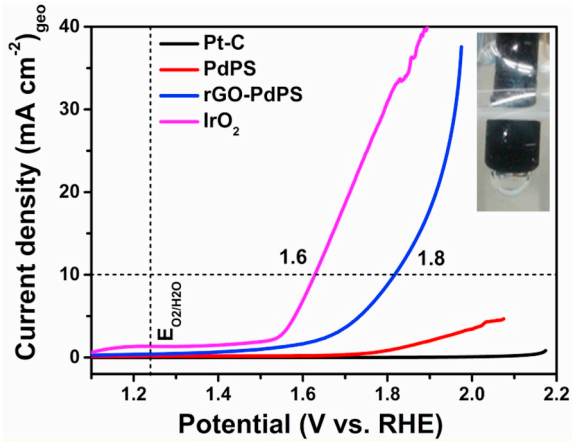

Fig. 4. Linear sweep voltammograms of oxygen evolution reaction on rGO-PdPS, PdPS, 40 wt % Pt-C and commercial IrO_2 in 1 M KOH electrolyte. Scan rate- 5 mVs^{-1}. Inset shows the digital image of oxygen bubble from the rGO-PdPS electrode during OER.

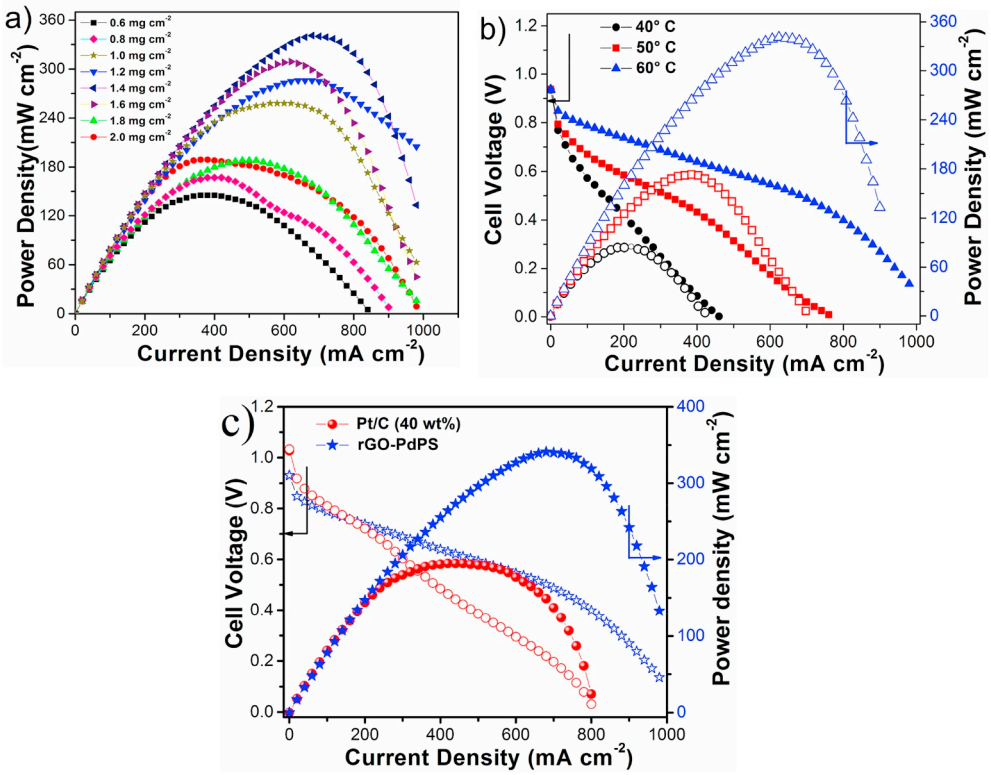

Fig. 3. (a) Power density plots for the optimization of the fuel cell performance by varying the rGO-PdPS loadings at the cathode. A constant 0.8 $mg_{Pt}cm^{-2}$ Pt loading for anode was maintained for all the fuel cells tested. (b) Polarization curves and power density profiles for analyzing the effect of operating temperatures. Closed symbols: Cell voltage vs. current density and opened symbols: Power density vs. current density. (c) Polarization curves and power density plots for AEMFCs comprising 1.4 $mgcm^{-2}$ rGO-PdPS and 0.8 $mg_{Pt}cm^{-2}$ Pt/C as cathode catalysts. Both cases anode loading was constant 0.8 $mg_{Pt}cm^{-2}$ Pt/C. The data was recorded at 60 °C.

and OER in alkaline medium.

The Tafel slopes (Fig. S8) for bulk PdPS and rGO-PdPS are determined to be 241 $mVdec^{-1}$ and 157 $mVdec^{-1}$, respectively. The observed high slope could be due to the formation of metal oxide or uncompensated ohmic drop or oxygen gas evolution from the electrode surface that blocks the electroactive sites for further reaction [51]. Continuous oxygen gas bubbles emanating from the electrode surface could reduce the electrocatalytic activity with time. The durability of the catalysts is evaluated by continuously cycling the potential as shown in Fig. S9. After several hundred cycles, a reduction of ~30% from the initial current density is observed implying that the catalyst, rGO-PdPS is stable for OER in alkaline medium. The reduction in current may be due to physical removal of the catalyst due to bubble formation. The enhancement of the catalytic activity of rGO-PdPS composite can also be anticipated based on high d band density of states near the Fermi level. The electron density of states (DOS) close to the Fermi level is correlated to the adsorbate– substrate adsorption energy based on the interactions between d-band electrons of the metal and those of the adsorbate. As a result, the d-band DOS should influence the adsorption strength and catalytic activity of the metal surface. It is found that the DOS of PdPS is close to Fermi energy [52] and this is one of the reasons for its electrocatalytic activity. It is likely that the presence of rGO may lead to strong hybridization between metal d-orbitals and π-orbital of the rGO, resulting in shifting of the d-band density towards Fermi energy [53,54]. Suntivich and co-workers [55] have shown that the e_g orbital of transition metal ions forms σ bonding with surface anion adsorbents, and as a result, the bond strength of O_2-related intermediate species on the catalytic surface changes. Synergetic coupling effect between the catalyst (Co_3O_4 and Ni_3S_2) and the support (Au, graphene, Ni foam) [36,56] has been invoked to explain the catalytic behavior.

4. Conclusions

The present study introduces a phosphochalcogenide electrocatalyst based on ternary PdPS and its rGO composite as an efficient electrocatalyst towards ORR in alkali medium. ORR activity is observed to be very close to Pt/C that is reflected in the difference in half-wave potential value, i.e. 30 mV. The RDE/RRDE studies reveal that the composite material reduces molecular oxygen by four electron transfer pathway and exhibits high methanol tolerant behavior. The catalyst used as cathode in AEMFCs shows a significant peak power density of about 341 $mWcm^{-2}$ at loading of 1.4 $mgcm^{-2}$ at 60 °C.

CRediT authorship contribution statement

Sujoy Sarkar: Writing - original draft. **Shubham Patel:** Writing - original draft. **S. Sampath:** Writing - original draft.

Acknowledgements

This work is supported by DST, India. Sujoy thanks CSIR, India for research fellowship.

Appendix A. Supplementary data

Supplementary data to this article can be found online at https://doi.org/10.1016/j.jpowsour.2019.227280.

References

[1] M. Winter, J.R. Brodd, Chem. Rev. 104 (2004) 4245.
[2] B.C.H. Steele, A. Heinzel, Nature 414 (2001) 345.
[3] A.A. Gewirth, M.S. Thorum, Inorg. Chem. 49 (2010) 3557.
[4] A.J. Appleby, J. Electroanal. Chem. 357 (1993) 117.
[5] O.J. Murphy, S. Srinivasan, B.E. Conway, *E*lectrochemistry in Transition: from the 20t^h to the 21s^t Century, Springer US, Boston, MA, 1992, p. 107.
[6] A. Kirubakaran, S. Jain, R.K. Nema, Renew. Sustain. Energy Rev. 13 (2009) 2430.
[7] J.R. Varcoe, P. Atanassov, D.R. Dekel, A.M. Herring, M.A. Hickner, P.A. Kohl, A. R. Kucernak, W.E. Mustain, K. Nijmeijer, K. Scott, T. Xu, L. Zhuang, Energy Environ. Sci. 7 (2014) 3135.
[8] S. Gottesfeld, D.R. Dekel, M. Page, C. Bae, Y. Yan, P. Zelenay, Y.S. Kim, J. Power. Sources 375 (2018) 170.
[9] N.M. Marković, T.J. Schmidt, V. Stamenković, P.N. Ross, Fuel Cells 1 (2001) 105.
[10] P.P. Lopes, D. Tripkovic, P.F.B.D. Martins, D. Strmcnik, E.A. Ticianelli, V. R. Stamenkovic, N.M. Markovic, J. Electroanal. Chem. 819 (2017) 123.
[11] M. Shao, Q. Chang, J.-P. Dodelet, R. Chenitz, Chem. Rev. 116 (2016) 3594.
[12] M. Lefèvre, E. Proietti, F. Jaouen, J.-P. Dodelet, Science 324 (2009) 71.
[13] Z. Chen, D. Higgins, A. Yu, L. Zhang, J. Zhang, Energy Environ. Sci. 4 (2011) 3167.
[14] V. Kiran, K. Srinivasu, S. Sampath, Phys. Chem. Chem. Phys. 15 (2013) 8744.
[15] Y. Liu, T.G. Kelly, J.G. Chen, W.E. Mustain, ACS Catal. 3 (2013) 1184.
[16] W. Chu, D. Higgins, Z. Chen, R. Cai, Non-Noble Metal Fuel Cell Catalysts, Wiley-VCH Verlag GmbH & Co. KGaA, 2014, p. 357.
[17] X. Tian, J. Luo, H. Nan, Z. Fu, J. Zeng, S. Liao, J. Mater. Chem. 3 (2015) 16801.
[18] D. Ham, J. Lee, Energies 2 (2009) 873.
[19] N. Alonso-Vante, H. Tributsch, O. Solorza-Feria, Electrochim. Acta 40 (1995) 567.
[20] O. Solorza-Feria, K. Ellmer, M. Giersig, N. Alonso-Vante, Electrochim. Acta 39 (1994) 1647.
[21] N. Alonso-Vante, P. Bogdanoff, H. Tributsch, J. Catal. 190 (2000) 240.
[22] M.-R. Gao, Y.-F. Xu, J. Jiang, S.-H. Yu, Chem. Soc. Rev. 42 (2013) 2986.
[23] Y. Zhang, Q. Zhou, J. Zhu, Q. Yan, S.X. Dou, W. Sun, Adv. Funct. Mater. 27 (2017) 1702317.
[24] D. Mukherjee, S. Sampath, 2D Inorganic Materials beyond Graphene, World Scientific (Europe), 2017, p. 103.
[25] H. Wang, H. Dai, Chem. Soc. Rev. 42 (2013) 3088.
[26] A. Arunchander, S.G. Peera, A.K. Sahu, J. Power. Sources 353 (2017) 104.
[27] A. Arunchander, S.G. Peera, V.V. Giridhar, A.K. Sahu, J. Electrochem. Soc. 164 (2017) F71.
[28] A. Arunchander, S.G. Peera, A.K. Sahu, ChemElectroChem 4 (2017) 1544.
[29] T.A. Bither, P.C. Donohue, H.S. Young, J. Solid State Chem. 3 (1971) 300.
[30] W. Jeitschko, Acta Crystallogr. B 30 (1974) 2565.
[31] S. Sarkar, S. Sampath, Chem. Commun. 50 (2014) 7359.
[32] D. Mukherjee, P.M. Austeria, S. Sampath, ACS. Energy. Lett. 1 (2016) 367.
[33] S. Sarkar, D. Mukherjee, S. Sampath, J. Power. Sources 362 (2017) 80.
[34] R.N. Jenjeti, P.M. Austeria, S. Sampath, ChemElectroChem 3 (2016) 1392.
[35] P. Ramesh, S. Bhagyalakshmi, S. Sampath, J. Colloid Interface Sci. 274 (2004) 95.
[36] Y. Liang, Y. Li, H. Wang, J. Zhou, J. Wang, T. Regier, H. Dai, Nat. Mater. 10 (2011) 780.
[37] L.X. Jinli Qiao, L. Ding, S. Penghui, L. Zhang, R. Baker, J. Zhang Int. J. Electrochem. Sci. 8 (2013) 1189.
[38] K.J.J. Mayrhofer, D. Strmcnik, B.B. Blizanac, V. Stamenkovic, M. Arenz, N. M. Markovic, Electrochim. Acta 53 (2008) 3181.
[39] N.M. Markovic, I.M. Tidswell, P.N. Ross, Langmuir 10 (1994) 1.
[40] H.S. Wroblowa, P.Y. Chi, G. Razumney, J. Electroanal. Chem. 69 (1976) 195.
[41] A. Damjanovic, M.A. Genshaw, Electrochim. Acta 15 (1970) 1281.
[42] Q. Liu, J. Jin, J. Zhang, J.ACS Appl. Mater. Interfaces 5 (2013) 5002.
[43] Z.-G. Zhao, J. Zhang, Y. Yuan, H. Lv, Y. Tian, D. Wu, Q.-W. Li, Sci. Rep. 3 (2013) 2263.
[44] R. Li, Z. Wei, X. Gou, W. Xu, RSC Adv. 3 (2013) 9978.
[45] D.-S. Yang, D. Bhattacharjya, M.Y. Song, J.-S. Yu, Carbon 67 (2014) 736.
[46] J.P. Paraknowitsch, A. Thomas, Energy Environ. Sci. 6 (2013) 2839.
[47] D.-S. Yang, D. Bhattacharjya, S. Inamdar, J. Park, J.-S. Yu, J. Am. Chem. Soc. 134 (2012) 16127.
[48] Y. Gorlin, T.F. Jaramillo, J. Am. Chem. Soc. 132 (2010) 13612.
[49] D. Wang, X. Chen, D.G. Evans, W. Yang, Nanoscale 5 (2013) 5312.
[50] B.R. Wygant, K. Kawashima, C.B. Mullins, ACS Energy Lett 3 (2018) 2956.
[51] D.U. Lee, B.J. Kim, Z. Chen, J. Mater. Chem. 1 (2013) 4754.
[52] A. Hamidani, B. Bennecer, Comput. Mater. Sci. 48 (2010) 115.
[53] J. Ma, A. Habrioux, C. Morais, A. Lewera, W. Vogel, Y. Verde-Gómez, G. Ramos-Sanchez, P.B. Balbuena, N. Alonso-Vante, ACS Catal. 3 (2013) 1940.
[54] Y. Ma, Y. Dai, M. Guo, C. Niu, B. Huang, Nanoscale 3 (2011) 3883.
[55] J. Suntivich, K.J. May, H.A. Gasteiger, J.B. Goodenough, Y. Shao-Horn, Science 334 (2011) 1383.
[56] B.S. Yeo, A.T. Bell, J. Am. Chem. Soc. 133 (2011) 5587.